Synthesis, Structure, and Electronic Properties of Monomeric and Dimeric Trispyrazolylborate Platinum(II) Hydride Complexes

Stefan Reinartz, Mu-Hyun Baik, Peter S. White, Maurice Brookhart,* and Joseph L. Templeton*

Department of Chemistry, University of North Carolina at Chapel Hill, Chapel Hill, North Carolina 27599-3290

Received January 24, 2001

Tp′PtMe(H)$_2$ (**2**) [Tp′ = hydridotris(3,5-dimethylpyrazolyl)borate] has been prepared from Tp′PtMe(CO) (**1**) via reaction with water in a basic acetone/water mixture. Protonation of **2** at one of the pyrazole nitrogen atoms induces methane elimination, and the resulting platinum(II) monohydride solvent intermediate (**3**) can be trapped by added ligand. Two chiral cationic platinum(II) monohydride complexes of the type [κ^2-((Hpz*)BHpz*$_2$)Pt(H)(L)][BAr′$_4$] [L = MeCN (**4**), CH_2═CH_2 (**5**); pz* = 3,5-dimethylpyrazolyl, BAr′$_4$ = tetrakis(3,5-trifluoromethylphenyl)borate] have been isolated. If **2** is protonated in the absence of trapping ligand, a deep red hydride-bridged dinuclear complex, [κ^2-((Hpz*)BHpz*$_2$)Pt(μ-H)]$_2$[BAr′$_4$]$_2$ (**6**), forms. DFT calculations supplement intuitive expectations regarding 3-center-2-electron bridging orbital descriptions for the electronic structure of this complex. X-ray structure determinations for the monomeric acetonitrile adduct **4** and the dicationic dimer **6** are reported.

Introduction

Bimetallic complexes with bridging hydride ligands display diverse structural and spectroscopic features. Dimeric hydride-bridged platinum complexes in particular have been extensively studied since the mid 1970s, and they exhibit a plethora of structural types. Neutral, doubly hydride bridged compounds [{Pt(μ-H)(SiR_3)(PR'_3)}]$_2$ (**A** in Figure 1) were early Pt(II) examples.[1,2] A large group of dimeric platinum complexes with bridging hydride ligands contains the $[Pt_2H_nP_4]^{m+}$ (n = 1−3; m = 1,2) core (e.g., **B**−**D** in Figure 1).[3−35] These compounds are doubly hydride bridged and stabilized by monophosphine[3−7] or diphosphine ligands[8−15] or else they are singly hydride bridged and again stabilized by monophosphine[16−20] or diphosphine ligands.[21−23] Spencer's dimeric complexes containing the $[Pt_2H_2(P\cap P)_2]^{2+}$ core (**C** in Figure 1),[14,15] which are yellow or red, are particularly relevant since they are direct analogues of the dicationic, N-supported dihydride-bridged dimer reported in this paper. The second large group of complexes contains mixed bridging ligands consisting of a hydride and a carbon,[11,24] sulfur,[25] phosphido,[26−29] or phosphine bridging ligand.[30−35] "A-frame" complexes are the principal subgroup in this set (**E** in Figure 1).[31−35] Platinum(I), 30-electron species of the general

(1) Green, M.; Howard, J. A. K.; Proud, J.; Spencer, J. L.; Stone, F. G. A.; Tsipis, C. A. *J. Chem. Soc., Chem. Commun.* **1976**, 671.
(2) Ciriano, M.; Green, M.; Howard, J. A. K.; Proud, J.; Spencer, J. L.; Stone, F. G. A.; Tsipis, C. A. *J. Chem. Soc., Dalton Trans.* **1978**, 801.
(3) Bracher, G.; Grove, D. M.; Pregosin, P. S.; Venanzi, L. M. *Angew. Chem., Int. Ed. Engl.* **1979**, *18*, 155.
(4) Paonessa, R. S.; Trogler, W. C. *J. Am. Chem. Soc.* **1982**, *104*, 3529.
(5) Bachechi, F.; Bracher, G.; Grove, D. M.; Kellenberger, B.; Pregosin, P. S.; Venanzi, L. M.; Zambonelli, L. *Inorg. Chem.* **1983**, *22*, 1031.
(6) Paonessa, R. S.; Trogler, W. C. *Inorg. Chem.* **1983**, *22*, 1038.
(7) Packett, D. L.; Syed, A.; Trogler, W. C. *Organometallics* **1988**, *7*, 159.
(8) Knobler, C. B.; Kaesz, H. D.; Minghetti, G.; Bandini, A. L.; Banditelli, G.; Bonati, F. *Inorg. Chem.* **1983**, *22*, 2324.
(9) Chiang, M. Y.; Bau, R.; Minghetti, G.; Bandini, A. L.; Banditelli, G.; Koetzle, T. F. *Inorg. Chem.* **1984**, *23*, 122.
(10) Carmichael, D.; Hitchcock, P. B.; Nixon, J. F.; Pidcock, A. *J. Chem. Soc., Chem. Commun.* **1988**, 1554.
(11) Bandini, A. L.; Banditelli, G.; Cinellu, M. A.; Sanna, G.; Minghetti, G.; Demartin, F.; Manassero, M. *Inorg. Chem.* **1989**, *28*, 404.
(12) Aime, S.; Gobetto, R.; Bandini, A. L.; Banditelli, G.; Minghetti, G. *Inorg. Chem.* **1991**, *30*, 316.
(13) Haggerty, B. S.; Housecroft, C. E.; Rheingold, A. L.; Shaykh, B. A. M. *J. Chem. Soc., Dalton Trans.* **1991**, 2175.
(14) Crascall, L. E.; Spencer, J. L. *J. Chem. Soc., Dalton Trans.* **1995**, 2391.
(15) Mole, L.; Spencer, J. L.; Litster, S. A.; Redhouse, A. D.; Carr, N.; Orpen, A. G. *J. Chem. Soc., Dalton Trans.* **1996**, 2315.
(16) Bracher, G.; Grove, D. M.; Venanzi, L. M,; Bachechi, F.; Mura, P.; Zambonelli, L. *Angew. Chem., Int. Ed. Engl.* **1978**, *17*, 778.
(17) Carmona, D.; Chaloupka, S.; Jans, J.; Thouvenot, R.; Venanzi, L. M. *J. Organomet. Chem.* **1984**, *275*, 303.
(18) Bachechi, F. *Acta Crystallogr.* **1993**, *C49*, 460.
(19) Bachechi, F.; Mura, P.; Zambonelli, L. *Acta Crystallogr.* **1993**, *C49*, 2072.
(20) Albinati, A.; Chaloupka, S.; Eckert, J.; Venanzi, L. M.; Wolfer, M. K. *Inorg. Chim. Acta* **1997**, *259*, 305.
(21) Minghetti, G.; Banditelli, G.; Bandini, A. L. *J. Organomet. Chem.* **1977**, *139*, C80.
(22) Tulip, T. H.; Yamagata, T.; Yoshida, T.; Wilson, R. D.; Ibers, J. A.; Otsuka, S. *Inorg. Chem.* **1979**, *18*, 2239.
(23) Rimml, H.; Venanzi, L. M. *J. Organomet. Chem.* **1984**, *260*, C52.
(24) Ara, I.; Falvello, L. R.; Forniés, J.; Lalinde, E.; Martín, A.; Martínez, F.; Moreno, M. T. *Organometallics* **1997**, *16*, 5392.
(25) Clegg, W.; Capdevila, M.; Gonzaléz-Duarte, P.; Sola, J. *Acta Crystallogr.* **1996**, *B52*, 270.
(26) Goel, A. B.; Goel, S. *Inorg. Chim. Acta* **1984**, *90*, L33.
(27) Leoni, P.; Manetti, S.; Pasquali, M. *Inorg. Chem.* **1995**, *34*, 749.
(28) Leoni, P.; Pasquali, M.; Fortunelli, A.; Germano, G.; Albinati, A. *J. Am. Chem. Soc.* **1998**, *120*, 9564.
(29) Leoni, P.; Pasquali, M.; Cittadini, V.; Fortunelli, A.; Selmi, M. *Inorg. Chem.* **1999**, *38*, 5257.
(30) Dillinger, K.; Oberhauser, W.; Bachman, C.; Brüggeller, P. *Inorg. Chim. Acta* **1994**, *223*, 13.
(31) Brown, M. P.; Puddephatt, R. J.; Rashidi, M.; Seddon, K. R. *Inorg. Chim. Acta* **1977**, *23*, L27.
(32) Brown, M. P.; Puddephatt, R. J.; Rashidi, M.; Seddon, K. R. *J. Chem. Soc., Dalton Trans.* **1978**, 516.
(33) Puddephatt, R. J.; Azam, K. A.; Hill, R. H.; Brown, M. P.; Nelson, C. D.; Moulding, R. P.; Seddon, K. R.; Grossel, M. C. *J. Am. Chem. Soc.* **1983**, *105*, 5642.
(34) Xu, C.; Anderson, G. K. *Organometallics* **1994**, *13*, 3981.
(35) Xu, C.; Anderson, G. K. *Organometallics* **1996**, *15*, 1760.

10.1021/ic010099q CCC: $20.00
Published on Web 07/28/2001

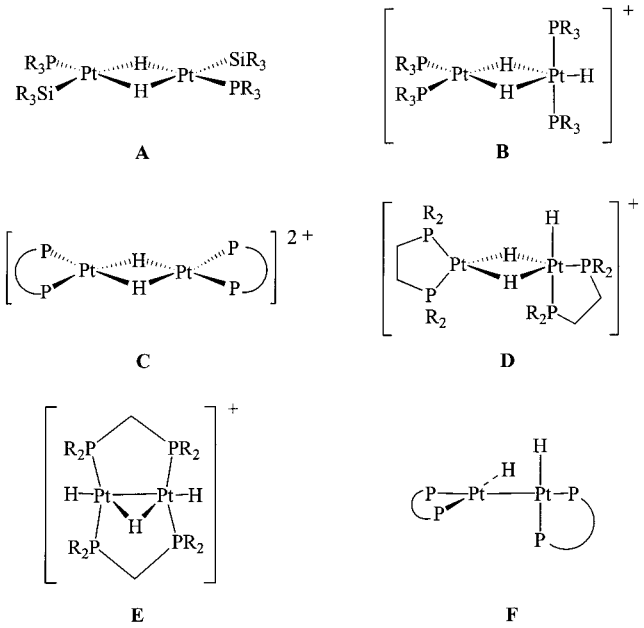

Figure 1. Examples of dimeric platinum complexes with bridging hydride ligands.

formula $[PtHP_2]_2$ (**F** in Figure 1) constitute a third group of complexes,[36−39] although hydride bridges in the ground state structure are only observed with electron-poor phosphines as supporting ligands.[39] Note that phosphines are the prevalent supporting ligands in these hydride-bridged dinuclear species. Few dimeric hydrido platinum complexes contain nitrogen-donor ligands in the platinum coordination sphere.[40−44]

The chemistry of TpPt(R)(R′)H [Tp = hydridotris(pyrazolyl)-borate; Tp′ = hydridotris(3,5-dimethylpyrazolyl)borate; R, R′ = combinations of alkyl, hydride, and aryl groups] has been extensively studied.[45−49] The stability of these complexes stems from tridentate coordination of the tris(pyrazolyl)borate ligand,[50] which anchors the octahedral coordination sphere of the platinum(IV) center and inhibits formation of a five-coordinate platinum(IV) intermediate which is on the pathway for reductive elimination.[51−61] On the other hand, low-temperature protonation induces reductive elimination of methane from Tp′PtMe$_2$H under mild conditions, leading to cationic platinum(II) complexes of the type [κ^2-((Hpz*)BHpz*$_2$)Pt(Me)(L)][BAr′$_4$] [L = trapping ligand; pz* = 3,5-dimethylpyrazolyl, BAr′$_4$ = tetrakis(3,5-trifluoromethylphenyl)borate] after addition of a trapping ligand.[62]

Haskel and Keinan recently reported synthesis of the unsubstituted pyrazolylborate complex TpPtMe(H)$_2$ from TpPtMe(CO) via reaction with water.[48] This transformation caught our attention since an analogous Tp′PtMe(H)$_2$ complex would potentially provide a route into the chemistry of cationic platinum(II) monohydride complexes analogous to the cationic platinum(II) methyl and phenyl complexes.[62] Following the synthesis of Tp′PtMe(H)$_2$ (**2**) from Tp′PtMe(CO) (**1**), we now report protonation reactions of this dihydridoplatinum(IV) reagent with the acid [H(OEt$_2$)$_2$][BAr′$_4$].[63] Protonation of **2** followed by addition of a trapping ligand yields Pt(II) adducts. Protonation of **2** in methylene chloride solution without addition of a trapping ligand leads to the formation of an unusual deep red dimeric platinum complex, [κ^2-((Hpz*)BHpz*$_2$)Pt(μ-H)]$_2$-[BAr′$_4$]$_2$ (**6**). In order to understand the origin of the intense visible absorptions of the dimeric product, we have undertaken a DFT study of the electronic structure of this dimeric species. The electronic structure of transition metal complexes with bridging hydride ligands has previously been subjected to symmetry considerations[64] and EHMO,[65,66] Fenske−Hall,[67] and DFT calculations.[68, 69]

Experimental Section

Materials and Methods. Reactions were performed under an atmosphere of dry nitrogen or argon using standard Schlenk and drybox techniques. Argon and nitrogen were purified by passage through columns of BASF R3-11 catalyst and 4 Å molecular sieves. All glassware was oven dried before use. Methylene chloride, acetonitrile, and pentanes were purified under an argon atmosphere by passage through a column packed with activated alumina.[70] Deuterated methylene chloride was vacuum transferred from calcium hydride and degassed by several freeze−pump−thaw cycles. Tp′PtMe(CO)[62] and [H(OEt$_2$)$_2$][BAr′$_4$][63] were synthesized according to published procedures.

^{1}H and ^{13}C NMR spectra were recorded on a Bruker Avance 400 spectrometer. ^{1}H NMR and ^{13}C NMR chemical shifts were referenced to residual ^{1}H and ^{13}C signals of the deuterated solvents. UV/vis spectra

(36) Schwartz, D. J.; Andersen, R. A. *J. Am. Chem. Soc.* **1995**, *117*, 4014.
(37) Fryzuk, M. D.; Clentsmith, G. K. B.; Leznoff, D. B.; Rettig, S. J.; Geib, S. J. *Inorg. Chim. Acta* **1997**, *265*, 169.
(38) Millar, S. P.; Jang, M.; Lachiotte, R. J.; Eisenberg, R. *Inorg. Chim. Acta* **1998**, *270*, 363.
(39) Bennett, B. L.; Roddick, D. M. *Inorg. Chem.* **1996**, *35*, 4703.
(40) Grove, D. M.; van Koten, G.; Ubbels, H. J. C.; Spek, A. L. *J. Am. Chem. Soc.* **1982**, *104*, 4285.
(41) Terheijden, J.; van Koten, G.; Grove, D. M.; Vrieze, K.; Spek, A. L. *J. Chem. Soc., Dalton Trans.* **1987**, 1359.
(42) Minghetti, G.; Cinellu, M. A.; Stoccoro, S.; Chelucci, G.; Zucca, A. *Inorg. Chem.* **1990**, *29*, 5138.
(43) Hill, G. S.; Puddephatt, R. J. *J. Am. Chem. Soc.* **1996**, *118*, 8745.
(44) Hill, G. S.; Vittal, J. J.; Puddephatt, R. J. *Organometallics* **1997**, *16*, 1209.
(45) O'Reilly, S. A.; White, P. S.; Templeton, J. L. *J. Am. Chem. Soc.* **1996**, *118*, 5684.
(46) Canty, A. J.; Dedieu, A.; Jin, H.; Milet, A.; Richmond, M. K. *Organometallics* **1996**, *15*, 2845.
(47) Wick, D. D.; Goldberg, K. I. *J. Am. Chem. Soc.* **1997**, *119*, 10235.
(48) Haskel, A.; Keinan, E. *Organometallics* **1999**, *18*, 4677.
(49) Wick, D. D.; Goldberg, K. I. *J. Am. Chem. Soc.* **1999**, *121*, 11900.
(50) Trofimenko, S. *Scorpionates—The Coordination Chemistry of Polypyrazolylborate Ligands*; Imperial College Press: London, 1999.
(51) Bartlett, K. L.; Goldberg, K. I.; Thatcher Bordon, W. *J. Am. Chem. Soc.* **2000**, *122*, 1456.
(52) Crumpton, D. M.; Goldberg, K. I. *J. Am. Chem. Soc.* **2000**, *122*, 962.
(53) Williams, B. S.; Holland, A. W.; Goldberg, K. I. *J. Am. Chem. Soc.* **1999**, *121*, 252.
(54) Goldberg, K. I.; Yan, J. Y.; Breitung, E. M. *J. Am. Chem. Soc.* **1995**, *117*, 6889.
(55) Hill, G. S.; Yap, G. P. A.; Puddephatt, R. J. *Organometallics* **1999**, *18*, 1408.
(56) Hill, G. S.; Puddephatt, R. J. *Organometallics* **1998**, *17*, 1478.
(57) Hill, G. S.; Puddephatt, R. J. *Organometallics* **1997**, *16*, 4522.
(58) Jenkins, H. A.; Yap, G. P. A.; Puddephatt, R. J. *Organometallics* **1997**, *16*, 1946.
(59) Roy, S.; Puddephatt, R. J.; Scott, J. D. *J. Chem. Soc., Dalton Trans.* **1989**, 2121.
(60) Brown, M. P.; Puddephatt, R. J.; Upton, C. E. E. *J. Chem. Soc., Dalton Trans.* **1974**, 2457.
(61) Fekl, U.; Zahl, A.; van Eldik, R. *Organometallics* **1999**, *18*, 4156.
(62) Reinartz, S.; White, P. S., Brookhart, M.; Templeton, J. L. *Organometallics* **2000**, *19*, 3854.
(63) M. Brookhart, B. Grant, A. F., Volpe, Jr. *Organometallics* **1992**, *11*, 3920.
(64) Cotton, F. A.; Daniels, L. M.; Jordan, G. T., IV; Lin, C.; Murillo, C. A. *J. Am. Chem. Soc.* **1998**, *120*, 3398.
(65) Dedieu, A.; Albright, T. A.; Hoffmann, R. *J. Am. Chem. Soc.* **1979**, *101*, 3141.
(66) Miller, R. L.; Lawler, K. A.; Bennett, J. L.; Wolczanski, P. T. *Inorg. Chem.* **1996**, *35*, 3242.
(67) Jezowska-Trzebiatowska, B.; Nissen-Sobocinska, B. *J. Organomet. Chem.* **1987**, *322*, 331.
(68) Fryzuk, M. D.; Johnson, S. A.; Rettig, S. J. *Organometallics* **2000**, *19*, 3931.
(69) Fryzuk, M. D.; Johnson, S. A.; Patrick, B. O.; Albinati, A.; Mason, S. A.; Koetzle, T. F. *J. Am. Chem. Soc.* **2001**, *123*, 3960.
(70) Pangborn, A. B.; Giardello, M. A.; Grubbs, R. H.; Rosen, R. K.; Timmers, F. J. *Organometallics* **1996**, *15*, 1518.

were recorded on a Hewlett-Packard 8452A diode array spectrophotometer, and infrared spectra were recorded on an ASI ReactIR 1000. Chemical analyses were performed by Atlantic Microlabs of Norcross, GA.

Tp′Pt(CH$_3$)(H)$_2$ (2). Tp′Pt(CH$_3$)(CO) (200 mg, 0.37 mmol) was added to 40 mL of a 1:1 acetone/water mixture to which 2 drops of 50% NaOH solution had been added. The reaction mixture was heated to a gentle reflux for 4 h. The resulting white precipitate was filtered through a glass frit and dried in vacuo. Product **2** (175 mg) was collected as a white solid. Tp′Pt(CH$_3$)(D)$_2$ (**2**-d_2) was synthesized in an analogous fashion in acetone-d_6/D$_2$O. Yield: 92%. IR (KBr): ν_{BH} = 2517 cm^{-1}, ν_{PtH} = 2247 cm^{-1}. ^{1}H NMR (CD$_2$Cl$_2$, δ): 5.86 (s, 2H, $^4J_{Pt-H}$ = 6.0 Hz, Tp′C*H*), 5.79 (s, 1H, $^4J_{Pt-H}$ = 6.8 Hz, Tp′C*H*), 2.39, 2.33, 2.26, 2.08 (s, 6H, 3H, 6H, 3H, Tp′CH_3), 1.02 (s, 3H, $^2J_{Pt-H}$ = 65 Hz, Pt−CH_3), −19.97 (s, 2H, $^1J_{Pt-H}$ = 1260 Hz, Pt−*H*). ^{13}C NMR (CD$_2$Cl$_2$, δ): 150.0 (2C, J_{Pt-C} = 23 Hz, Tp′*C*CH$_3$), 149.3 (1C, J_{Pt-C} = 24 Hz, Tp′*C*CH$_3$), 144.73, 144.66 (2C, 1C, Tp′*C*CH$_3$), 106.3 (2C, $^3J_{Pt-C}$ = 10 Hz, Tp′*C*H), 105.3 (1C, $^3J_{Pt-C}$ = 10 Hz, Tp′*C*H), 15.8 (1C, J_{Pt-C} = 32 Hz, Tp′*C*H$_3$), 14.3 (2C, J_{Pt-C} = 14 Hz, Tp′*C*H$_3$), 12.7 (3C, Tp′*C*H$_3$), −32.5 ($^1J_{Pt-C}$ = 570 Hz, Pt−*C*H$_3$). Anal. Calcd For C$_{16}$H$_{27}$N$_6$BPt: C, 37.73; H, 5.34; N, 16.50. Found: C, 37.83; H, 5.24; N, 16.50.

Representative [BAr′$_4$]$^-$ NMR Data. ^{1}H and ^{13}C NMR data for the [BAr′$_4$]$^-$ counterion are reported separately for simplicity. ^{1}H NMR (CD$_2$Cl$_2$, δ): 7.77 (br, 8H, *o*-Ar′), 7.60 (br, 4H, *p*-Ar′). ^{13}C NMR (CD$_2$Cl$_2$, δ): 162.2 (1:1:1:1 pattern, $^1J_{B-C}$ = 50 Hz, C$_{ipso}$), 135.3 (C$_{ortho}$), 129.4 (qq, $^2J_{C-F}$ = 30 Hz, $^4J_{C-F}$ = 5 Hz, C$_{meta}$), 125.1 (q, $^1J_{C-F}$ = 270 Hz, *C*F$_3$), 117.9 (C$_{para}$).

Protonation of Tp′Pt(CH$_3$)(H)$_2$ (2). Equimolar amounts of Tp′Pt(CH$_3$)(H)$_2$ (**2**) and [H(OEt$_2$)$_2$][BAr′$_4$] were weighed into an NMR tube in an argon-filled drybox. The NMR tube was then sealed with a septum and secured with Teflon tape. The sample was cooled to −78 °C outside the drybox, and about 0.6 mL of CD$_2$Cl$_2$ was slowly added through the septum. **3**: ^{1}H NMR (CD$_2$Cl$_2$, 193K, δ): 11.55 (s, 1H, pz*N*H*), 6.11, 5.99, 5.97 (s, 1H each, HTp′C*H*), 2.31, 2.29, 2.28, 2.15, 2.10, 1.73 (s, 3H each, HTp′CH_3), −22.49 (s, 1H, $^1J_{Pt-H}$ = 1053 Hz, Pt−*H*), 0.14 (s, C*H*$_4$). ^{13}C NMR (CD$_2$Cl$_2$, 193K, δ): 153.3, 152.5, 149.1, 148.72, 148.68, 144.4 (HTp′*C*CH$_3$), 109.7, 108.1, 107.8 (HTp′*C*H), 17.6, 14.3, 14.1, 13.7, 12.2, 12.0 (HTp′*C*H$_3$).

[κ^2-((Hpz*)BHpz*$_2$)Pt(H)(NCCH$_3$)][BAr′$_4$] (4). Tp′Pt(CH$_3$)(H)$_2$ (45 mg, 0.088 mmol) and [H(OEt$_2$)$_2$][BAr′$_4$] (90 mg, 1 equiv) were combined in a Schlenk flask and cooled to −78 °C. CH$_2$Cl$_2$ (15 mL) was slowly added through the septum. The reaction mixture was stirred for ca. 5 min (a pink color appeared), and then 5 mL of CH$_3$CN was added. The reaction mixture was allowed to warm to ambient temperature. The solvent was removed in vacuo, and the residue was triturated with pentane. Colorless crystals, as well as some noncrystalline material, were obtained from CH$_2$Cl$_2$/pentane at −30 °C. Yield: 72 mg (58%). IR (KBr): ν_{PtH} = 2200 cm^{-1}. ^{1}H NMR (CD$_2$Cl$_2$, δ): 12.86 (br, 1H, pz*N*H*), 6.14, 6.02, 6.01 (s, 1H each, HTp′C*H*), 2.40, 2.36, 2.34, 2.32, 2.30, 2.22 (s, 3H, 6H, 3H, 3H, 3H, 3H, HTp′CH_3 and Pt−NCCH_3), −20.02 (s, 1H, $^1J_{Pt-H}$ = 1202 Hz, Pt−*H*). ^{13}C NMR (CD$_2$Cl$_2$, δ): 154.0, 152.2, 149.7, 148.6, 147.8, 144.0 (HTp′*C*CH$_3$), 108.7, 108.2, 107.8 (HTp′*C*H), 17.2, 13.9, 13.7, 13.2, 12.6, 11.3 (HTp′*C*H$_3$), 4.1 (Pt−NC*C*H$_3$). Anal. Calcd For C$_{49}$H$_{39}$N$_7$B$_2$F$_{24}$Pt: C, 42.08; H, 2.81; N, 7.01. Found: C, 42.23; H, 2.78; N, 6.73.

[κ^2-((Hpz*)BHpz*$_2$)Pt(H)(CH$_2$=CH$_2$)][BAr′$_4$] (5). Tp′Pt(CH$_3$)(H)$_2$ (51 mg, 0.10 mmol) and [H(OEt$_2$)$_2$][BAr′$_4$] (104 mg, 1 equiv) were combined in a Schlenk flask and cooled to −78 °C. CH$_2$Cl$_2$ (15 mL) was slowly added through the septum. The reaction mixture was stirred for ca. 5 min (a pink color appeared), and then ethylene gas was purged through the solution while the reaction mixture was allowed to warm to ambient temperature. The solvent was removed in vacuo, and the residue was triturated with pentane. A light yellow solid was obtained after recrystallization from CH$_2$Cl$_2$/pentane at −30 °C. Yield: 109 mg (79%). IR (KBr): ν_{PtH} = 2235 cm^{-1}. ^{1}H NMR (CD$_2$Cl$_2$, 203K, δ): 10.59 (br, 1H, pz*N*H*), 6.10, 6.03, 5.96 (s, 1H each, HTp′C*H*), 3.86, 3.51 (m, 2H each, J_{Pt-H} = 56 Hz, Pt-bound ethylene), 2.32, 2.30, 2.24, 2.15, 1.57 (s, 3H, 3H, 6H, 3H, 3H, HTp′CH_3), −22.19 (s, 1H, $^1J_{Pt-H}$ = 1048 Hz, Pt−*H*); ^{13}C NMR (CD$_2$Cl$_2$, 203K, δ): 152.6, 152.4, 148.3, 148.0, 143.2 (HTp′*C*CH$_3$), 109.1, 107.8, 106.8 (HTp′*C*H), 60.4 ($^1J_{Pt-C}$ = 155 Hz, Pt-bound ethylene), 14.0, 13.9, 13.0, 12.8, 10.9, 10.7 (HTp′*C*H$_3$). Anal. Calcd for C$_{49}$H$_{40}$N$_6$B$_2$F$_{24}$Pt: C, 42.47; H, 2.91; N, 6.07. Found: C, 42.57; H, 3.05; N, 5.98.

Table 1. Crystallographic Data Collection Parameters

	4	**6**
formula	C$_{49}$H$_{39}$B$_2$F$_{24}$N$_7$Pt	(C$_{51}$H$_{46}$B$_2$F$_{24}$N$_6$OPt)$_2$
mol wt	1398.55	2863.24
cryst syst	triclinic	triclinic
space group	$P\bar{1}$	$P\bar{1}$
a, Å	12.8129(4)	13.0550(6)
b, Å	13.0993(4)	13.0718(6)
c, Å	18.9928(6)	18.3242(8)
α, deg	78.741(1)	96.278(1)
β, deg	87.858(1)	106.327(1)
γ, deg	62.287(1)	102.242(1)
V, Å^3	2762.52(15)	2884.74(23)
Z	2	1
density calcd, Mg/m^3	1.681	1.648
F (000)	1370.75	1410.77
cryst dimens, mm	0.35 × 0.35 × 0.30	0.25 × 0.20 × 0.10
temp, °C	−100	−100
radiation (*λ*, Å)	Mo Kα (0.71073)	Mo Kα (0.71073)
2*θ* range, deg	3−60	3−50
μ, mm^{-1}	2.65	2.54
scan mode	*ω*	*ω*
total no. of reflns	46864	27750
total no. of unique reflns	16085	10104
no. of obsd data ($I > 2.5\sigma(I)$)	13812	8842
no. of refined params	803	767
R_F, %	0.041	0.039
R_w, %	0.043	0.045
R_I, %	0.027	0.039
GOF	1.6604	1.7382

[κ^2-((Hpz*)BHpz*$_2$)Pt(*μ*-H)]$_2$[BAr′$_4$]$_2$ (6). Tp′Pt(CH$_3$)(H)$_2$ (75 mg, 0.147 mmol) and [H(OEt$_2$)$_2$][BAr′$_4$] (150 mg, 1 equiv) were combined in a Schlenk flask and cooled to −78 °C. CH$_2$Cl$_2$ (12 mL) was slowly added through the septum. The reaction mixture was stirred for ca. 5 min (a pink color appeared), and the flask was stored in a freezer at −30 °C for 12 h. Dark purple needles formed, and these were collected and washed with pentanes. Yield: 129 mg (65%). ^{1}H NMR (CD$_2$Cl$_2$, δ): 10.83 (br, 1H, pz*N*H*), 6.37, 5.99 (s, 1H, 2H, HTp′C*H*), 2.47, 2.46, 2.01, 1.99 (s, 6H, 3H, 6H, 3H, HTp′CH_3), −21.57 (s, 1H, $^1J_{Pt-H}$ = 981 Hz, Pt−*H*). ^{13}C NMR (CD$_2$Cl$_2$, δ): 153.6, 151.0, 150.5, 145.4 (HTp′*C*CH$_3$), 110.4, 108.9 (HTp′*C*H), 16.1, 13.2, 11.9, 11.5 (HTp′*C*H$_3$). UV/vis (CH$_2$Cl$_2$): λ = 526 nm (ϵ = 3.8 × 10^2 M^{-1} cm^{-1}), λ = 406 nm (ϵ = 5.9 × 10^2 M^{-1} cm^{-1}). Anal. Calcd for C$_{94}$H$_{72}$N$_{12}$B$_4$F$_{48}$Pt$_2$: C, 41.58; H, 2.67; N, 6.19. Found: C, 41.86; H, 2.71; N, 6.12.

X-ray Crystallography. Single crystals of **4** and **6** were mounted on a glass fiber. Diffraction data were collected on a Bruker SMART diffractometer using the *ω*-scan mode. Refinement was carried out with the full-matrix least-squares method based on *F* (NRCVAX) with anisotropic thermal parameters for all non-hydrogen atoms. Hydrogen atoms were inserted in calculated positions and refined riding with the corresponding atom. Complete details of X-ray data collection are given in Table 1.

Computational Details. All calculations were performed using the DFT[71,72] based program DMol3 (version 4.1)[73]. The VWN[74] local exchange-correlation potential, augmented by exchange and correlation functionals as suggested by Perdew and Wang (PW91),[75] was employed self-consistently for the full geometry optimization. A set of "double numerical plus" (DNP) basis functions with a FINE mesh was used throughout the study, and all electrons were included (no frozen core). Relativistic calculations were performed with scalar first order corrections (Pauli Hamiltonian) including all electrons.

(71) Parr, R. G.; Yang, W. *Density Functional Theory of Atoms and Molecules*; Oxford University Press: New York, 1989.
(72) Ziegler, T. *Chem. Rev.* **1991**, *91*, 651.
(73) Delley, B. *J. Chem. Phys.* **1990**, *92*, 508. DMol3 is available from MSI in the Cerius2 program suite.
(74) Vosko, S. H.; Wilk, L.; Nusair, M. *Can. J. Phys.* **1980**, *58*, 1200.
(75) Perdew, J. P.; Wang, Y. *Phys. Rev. B* **1992**, *45*, 13244.

Scheme 1. Synthesis of Tp′PtMe(H)$_2$ (**2**)

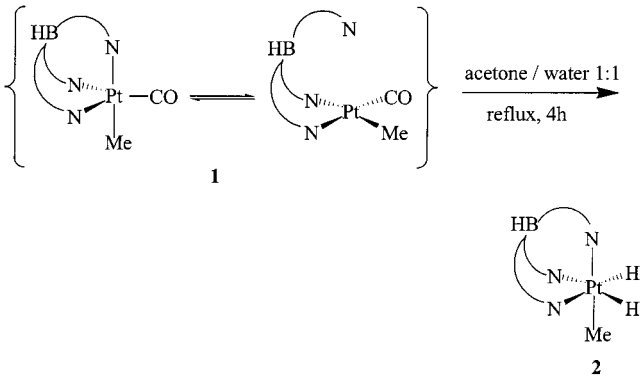

1 **2**

Results and Discussion

Synthesis of Tp′PtMe(H)$_2$. Haskel and Keinan recently reported the synthesis of TpPtMe(H)$_2$ from TpPtMe(CO) via reaction with water.[48] They suggested that nucleophilic attack on the CO ligand of TpPtMe(CO) by water was the first step in the overall transformation. We modified their procedure slightly by reacting the Tp′ analogue Tp′PtMe(CO) (**1**), which exists in solution in both square-planar and trigonal-bipyramidal geometries,[62] in acetone/water under basic conditions since this should accelerate the reaction. Gentle heating of **1** for 4 h in a 1:1 acetone/water solution, to which 2 drops of 50% NaOH had been added, results in the formation of Tp′PtMe(H)$_2$ (**2**), which is isolated after filtration as a white, air-stable powder in 92% yield (Scheme 1). In the absence of base the reaction was substantially slower and the yield decreased.

The solid state IR spectrum of Tp′PtMe(H)$_2$ **2** (KBr) shows an absorption at 2517 cm^{-1} for the B−H stretch of the Tp′ ligand, indicating κ^3 coordination,[76] and a broad absorption at 2247 cm^{-1} is assigned to the Pt−H stretches. A single IR absorption for the symmetric and antisymmetric modes implies the absence of strong vibrational coupling between the two hydride ligands, a common phenomena.[77−79] The ^{1}H NMR spectrum of **2** displays a 2:1 pattern for the resonances of the Tp′ ligand indicative of mirror symmetry, and the two equivalent hydrides resonate at −19.97 ppm ($^1J_{Pt-H}$ = 1260 Hz, ^{195}Pt, 33.4% abundant). The spectral features of **2** are congruent with data reported for TpPtH$_2$Me[48] and Tp′Pt(SiEt$_3$)(H)$_2$.[79]

Protonation of Tp′PtMe(H)$_2$. When the methyl dihydride complex **2** reacts with 1 equiv of the acid [H(OEt$_2$)$_2$][BAr′$_4$] in CD_2Cl_2 at −78 °C, methane formation (^{1}H NMR: δ = 0.14 ppm) is observed. No dihydrogen is detected. The ^{1}H NMR spectrum shows a single metal product with 1:1:1 patterns for the resonances of the Tp′ ligand, indicating a chiral metal center. An upfield resonance for a platinum-bound hydride is observed (δ = −22.49 ppm, $^1J_{Pt-H}$ = 1053 Hz), and a broad singlet at 11.55 ppm is assigned to the protonated pyrazole ring.[62,80−82] These NMR data are consistent with formation of the solvent (presumably diethyl ether) adduct, [κ^2-((Hpz*)BHpz*$_2$)Pt(H)(Solv)][BAr′$_4$] (**3**). Addition of excess MeCN or ethylene gas to the cationic platinum hydride intermediate at low temperatures cleanly affords the platinum(II) acetonitrile adduct [κ^2-((Hpz*)BHpz*$_2$)Pt(H)(NCMe)][BAr′$_4$] (**4**) or the platinum(II) ethylene adduct [κ^2-((Hpz*)BHpz*$_2$)Pt(H)(CH$_2$=CH$_2$)][BAr′$_4$] (**5**) (Scheme 2). Compounds **4** and **5** were obtained in preparatory scale syntheses in good yields as off-white, air-stable crystals.

If the methyl dihydride **2** is treated with deuterated acid, [D(OEt$_2$)$_2$][BAr′$_4$], no deuterium incorporation in the evolved methane is observed by ^{1}H NMR. Since the two hydride signals for the isotopomers [κ^2-((Dpz*)BHpz*$_2$)Pt(H)(Solv)][BAr′$_4$] (**3**-*d*) and [κ^2-((Hpz*)BHpz*$_2$)Pt(H)(Solv)][BAr′$_4$] (**3**) (present in about a 4:1 ratio) integrate for a total of one proton, deuterium incorporation into the hydride position is negligible. Hence, protonation of the methyl dihydride **2** occurs at a pyrazole ring rather than at either the metal or a methyl site. When Tp′PtMe(D)$_2$ (**2**-*d*$_2$) reacts with 1 equiv of [H(OEt$_2$)$_2$][BAr′$_4$], both CH_3D and CH_2D_2 are detected by ^{1}H NMR, and a substantial amount of hydrogen resides in the hydride position (ca. 0.6 H) of the product solvento complex **3**. Apparently, hydrogen scrambles from the methyl position into the hydride position, which implicates reversible formation of a σ-methane intermediate prior to methane loss. A plausible overall reaction sequence is protonation of Tp′PtMe(H)$_2$ (**2**) at a pyrazole ring with concomitant generation of an open coordination site in a five-coordinate platinum intermediate. Reversible reductive elimination of methane leads to a transient methane adduct, followed by methane loss and coordination of a solvent molecule. The solvent molecule is then displaced by either acetonitrile or ethylene.

The ^{1}H NMR spectrum of [κ^2-((Hpz*)BHpz*$_2$)Pt(H)(NCMe)][BAr′$_4$] (**4**) displays the N−*H* resonance of the protonated pyrazole ring at 12.86 ppm and the resonance for the hydride bound to platinum at −20.02 ppm ($^1J_{Pt-H}$ = 1202 Hz). The methyl carbon of the coordinated acetonitrile molecule resonates at 4.1 ppm.[62,83] The solid state IR spectrum of **3** (KBr) shows an absorption at 2200 cm^{-1} for the lone Pt−H stretch.

Single crystals of the hydrido acetonitrile complex **4** were subjected to X-ray structural analysis; an ORTEP diagram is shown in Figure 2. The hydride ligand on platinum could not be located in the difference Fourier map and was placed in a calculated position. This structure resembles the methyl analogue [κ^2-((Hpz*)BHpz*$_2$)PtMe(NCMe)][BAr′$_4$] with respect to bond lengths and the propeller disposition of the nitrogen heterocycles of the Tp′ ligand, leaving the protonated pyrazole nitrogen atom above the platinum square plane (see torsion angles). If the hydrogen bound to the pyrazole nitrogen atom is placed in a calculated position, a short Pt−H distance of 2.33 Å results, consistent with a 3-center-4-electron N−H−Pt bond.[84−86] Reflecting the strong trans influence of the hydride ligand, the Pt1−N21 distance trans to the hydride ligand of 2.133(3) Å is significantly longer (0.14 Å) than the Pt1−N11 distance of 1.985(2) Å trans to the acetonitrile ligand (Table 2).

The solid state IR spectrum of [κ^2-((Hpz*)BHpz*$_2$)Pt(H)(CH$_2$=CH$_2$)][BAr′$_4$] (**5**) (KBr) displays an absorption at 2235 cm^{-1} for the Pt−H stretch. The ^{1}H NMR spectrum shows

(76) Akita, M.; Ohta, K.; Takahashi, Y.; Hikichi, S.; Moro-oka, Y. *Organometallics* **1997**, *16*, 4121.
(77) L'Eplattenier, F.; Calderazzo, F. *Inorg. Chem.* **1967**, *6*, 2092.
(78) Girling, R. B.; Grebenik, P.; Perutz, R. N. *Inorg. Chem.* **1986**, *25*, 31.
(79) Reinartz, S.; White, P. S., Brookhart, M.; Templeton, J. L. *Organometallics* **2000**, *19*, 3748.
(80) Ball, R. G.; Ghosh, C. K.; Hoyano, J. K.; McMaster, A. D.; Graham, W. A. G. *J. Chem. Soc., Chem. Commun.* **1989**, 341.
(81) Rheingold, A. L.; Haggerty, B. S.; Trofimenko, S. *Angew. Chem., Int. Ed. Engl.* **1994**, *33*, 1983.
(82) Wiley: J. S.; Oldham, W. J. Jr.; Heinekey, D. M. *Organometallics* **2000**, *19*, 1670.
(83) Johansson, L.; Ryan, O. B.; Rømming, C.; Tilset, M. *Organometallics* **1998**, *17*, 3957.
(84) Brammer, L.; Zhao, D.; Ladipo, F. L.; Braddock-Wilking, J. *Acta Crystallogr.* **1995**, *B51*, 632.
(85) Albinati, A.; Lianza, F.; Pregosin, P. S.; Müller, B. *Inorg. Chem.* **1994**, *33*, 2522.
(86) Wehman-Ooyevaar, I. C. M.; Grove, D. M.; Kooijman, H.; van der Sluis, P.; Spek, A. L.; van Koten, G. *J. Am. Chem. Soc.* **1992**, *114*, 9916.

Scheme 2. Protonation of Tp′PtMe(H)$_2$ (**2**)

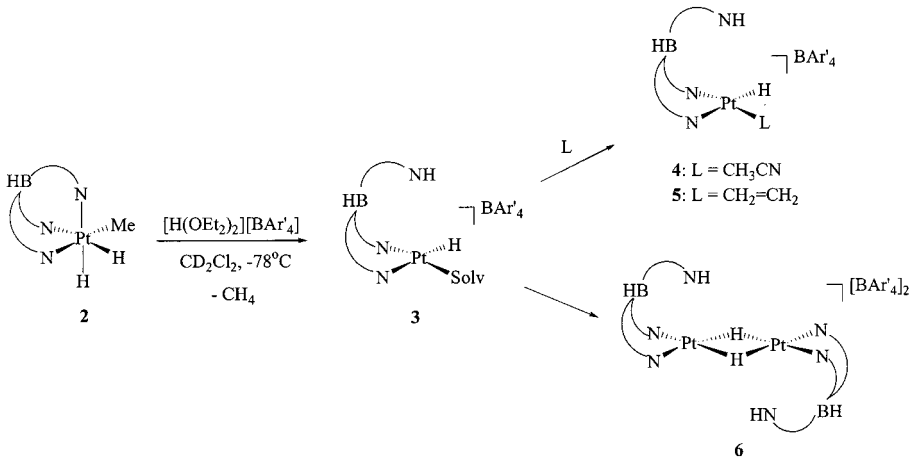

Table 2. Selected Bond Distances (Å) and Angles (deg) for Complex **4**

Pt1−N1	1.968(3)	N1−Pt1−N11	177.93(11)
Pt1−N11	1.985(2)	N1−Pt1−N21	94.63(10)
Pt1−N21	2.133(3)	N11−Pt1−N21	87.42(9)
Pt1−N31	3.173(3)	Pt1−N1−C2	178.1(3)
N1−C2	1.124(4)	N12−B10−N32−N31	−62.1 (5)
C2−C3	1.458(5)	N22−B10−N32−N31	62.7(5)

resonances at 10.1 ppm for the protonated pyrazole ring and at −22.19 ppm for the hydride ligand ($^1J_{Pt-H}$ = 1048 Hz). Two multiplets with broad platinum satellites (J_{Pt-H} = 69 Hz) integrating for two hydrogens each are observed between 3.5 and 4.0 ppm for the four protons of the coordinated ethylene molecule, indicating rapid rotation of the ethylene ligand about the midpoint of the ethylene−platinum bond on the NMR time scale at room temperature. Accordingly, both ethylene carbons resonate at 60.6 ppm ($^1J_{Pt-C}$ = 150 Hz) in the ^{13}C NMR spectrum.

Formation of a Hydride-Bridged Dimer. When Tp′PtMe(H)$_2$ (**2**) is protonated with [H(OEt$_2$)$_2$][BAr′$_4$] in CH_2Cl_2 without addition of trapping ligand, dark red-purple needles of X-ray quality form after standing overnight at −30 °C.[87] Single crystals of [κ^2-((Hpz*)BHpz*$_2$)Pt(μ-H)]$_2$[BAr′$_4$]$_2$ (**6**) were subjected to X-ray structural analysis; an ORTEP diagram is shown in Figure 3. The bridging hydride ligands could not be located in the difference Fourier map and were placed in calculated positions. The most important feature of this structure is the short Pt−Pt distance of 2.54 Å (Table 3), which is among the shortest distances reported for similar complexes. The two platinum square planes are almost coplanar, consistent with the assignment of a double hydride bridge to this dimeric species.

Table 3. Selected Bond Distances (Å) and Angles (deg) for Complex **6**

Pt1−Pt1a	2.5411(4)	N11−Pt1−N21	85.52(16)
Pt1−N11	2.006(4)	Pt1a−Pt1−N11	136.88(11)
Pt1−N21	2.005(4)	Pt1a−Pt1−N21	137.58(11)
		N12−B10−N32−N31	169.9(8)
		N22−B10−N32−N31	51.1(5)

The Tp′ resonances of complex **6** display a 2:1 pattern in both ^{1}H and ^{13}C NMR, indicating C_{2h} symmetry in solution. A hydride resonance at −21.57 ppm is observed in the ^{1}H NMR with very broad satellites ($^1J_{Pt-H}$ = 981 Hz), and the triplet for the bridging hydrides coupling to two spin active platinum centers can only be observed after extended acquisition times.[43] Presumably relaxation due to chemical shift anisotropy accounts for the difficulty in observing these satellites, each of which accounts for roughly 3% of the signal.[88] No IR absorption for the bridging hydride atoms was located, a common occurrence.[8,21,30,32] Although dimer **6** is stable for a period of months in the solid state at room temperature, it decomposes over a period of several hours in CH_2Cl_2 at room temperature.

The electronic spectrum (CH_2Cl_2) of the colorful dimeric complex **6** displays absorption maxima in the visible region at

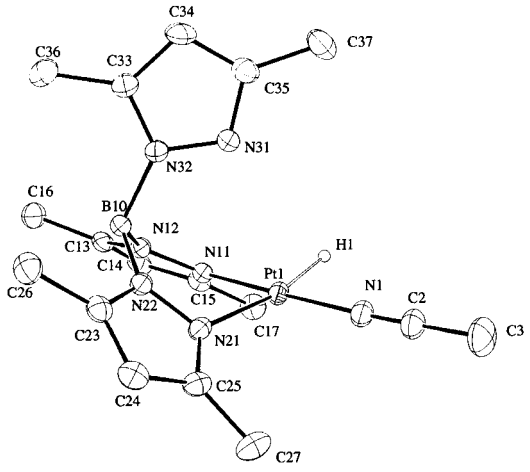

Figure 2. ORTEP diagram of [κ^2-((Hpz*)BHpz*$_2$)Pt(H)(NCMe)][BAr′$_4$] (**4**); ellipsoids are drawn at the 50% probability level, and the BAr′$_4$ counterion is omitted for clarity.

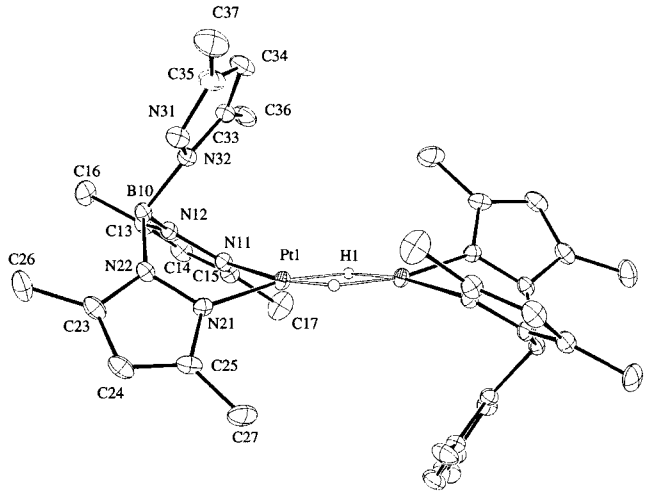

Figure 3. ORTEP diagram of [κ^2-((Hpz*)BHpz*$_2$)Pt(μ-H)]$_2$[BAr′$_4$]$_2$ (**6**); ellipsoids are drawn at the 50% probability level, and the BAr′$_4$ counterions are omitted for clarity.

Table 4. Distances and HOMO/LUMO Energies for the DFT-Optimized Structure of $[\kappa^2$-((Hpz)BHpz$_2$)PtH(NCMe)$]^+$ (**model-4**)

	Pt−H (Å)	Pt−N11 (Å)	Pt−N21 (Å)	Pt−N1 (Å)	N1−C2 (Å)	E^{LUMO} (eV)	E^{HOMO} (eV)
exptl (Table 2)		1.985	2.133	1.968	1.124		
DFT calcd, gas phase$_{rel}$	1.554	1.985	2.113	1.919	1.161	−5.38	−8.60

Table 5. Distances and HOMO/LUMO Energies for the DFT-Optimized Structure of $[\kappa^2$-((Hpz)BHpz$_2$)Pt(μ-H)$]_2^{2+}$ (**model-6**)

	Pt−Pt (Å)	Pt−H (Å)	Pt−N21 (Å)	E^{LUMO} (eV)	E^{HOMO} (eV)
exptl (Table 3)	2.541		2.005		
DFT calcd, gas phase$_{rel}$	2.542	1.748	1.998	−9.09	−10.93

406 nm ($\epsilon = 5.9 \times 10^2$ M^{-1} cm^{-1}) and 526 nm ($\epsilon = 3.8 \times 10^2$ M^{-1} cm^{-1}). Given the absence of comparable absorptions in related Pt(II) monomers, these absorptions prompted us to investigate the electronic structure of the dinuclear complex **6**. How does the electronic structure change upon going from a monomer (e.g., complex **4**) to a dimer (e.g., complex **6**)? Comparison of **6** with diborane, B_2H_6, provides a qualitative explanation for its deep red color. **6** is similar to B_2H_6 in that the coordinatively unsaturated metal centers complete their valences with bridging hydride ligands: the electronic structure thus approximates a simple 3-center-2-electron bond. The lowest energy transitions in such an orbital scheme will surely excite an electron to the central nonbonding MO of the 3-center-2-electron orbital. In a monomeric complex like **4**, such nonbonding levels are absent.

Geometry Optimization. To investigate the electronic description of dimer **6**, density functional theory (DFT) calculations were conducted. Geometrical parameters obtained after geometry optimization are listed in Tables 4 and 5. Model systems containing the protonated Tp ligand rather than Tp′ were employed in order to reduce the computational effort. The structural features of the calculated geometries for the monomeric acetonitrile adduct $[\kappa^2$-((Hpz)BHpz$_2$)PtH(NCMe)$]^+$ (**model-4**) and the hydride-bridged dimer $[\kappa^2$-((Hpz)BHpz$_2$)Pt(μ-H)$]_2^{2+}$ (**model-6**) are in good agreement with the X-ray structures of **4** and **6** only when relativistic corrections are included. The DFT calculations illustrate the trans influence of the hydride ligand in the monomeric system **model-4** evident from the X-ray structure of complex **4**: a Pt−N distance of 2.113 Å trans to the hydride is computed, which is significantly longer than the calculated Pt−N bond length of 1.985 Å trans to the acetonitrile ligand.

Electronic Spectroscopy. The computation of accurate excitation energies is a difficult task, often requiring multiconfigurational wave functions as available in the CASSCF level of theory.[89] Recently, time-dependent DFT has emerged as an alternative to expensive ab initio methods.[90,91] To achieve our limited goal of qualitatively understanding changes in the electronic structure upon dimerization of two Pt monomers, a more simple protocol was used. We approximate the excitation energies as the energy differences between the occupied and unoccupied Kohn−Sham orbitals responsible for the excitation. The intensity of the excitation is computed by numerically evaluating the transition dipole moments $\langle\psi(\text{occ})|x,y,z|\psi(\text{unocc})\rangle$, where ψ are the occupied and unoccupied Kohn−Sham orbitals. This is a severe approximation, and only qualitative agreement with experiment is expected.

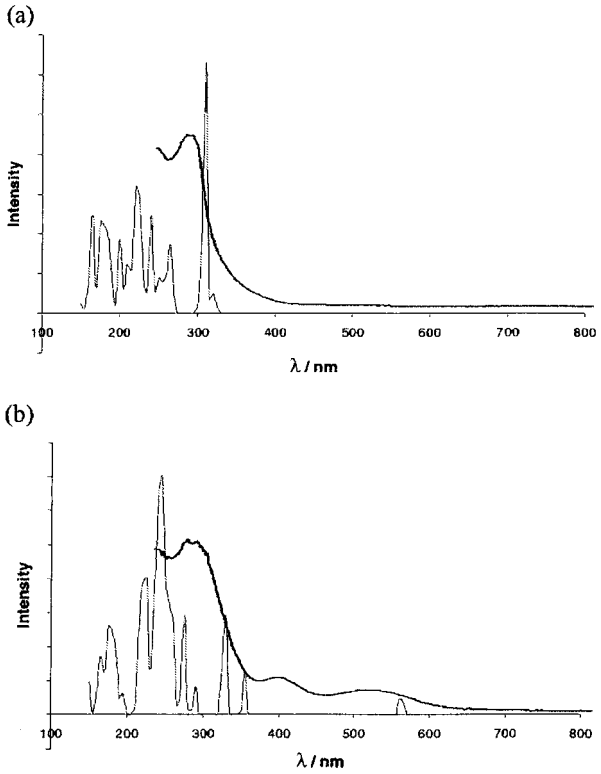

Figure 4. (a) Experimental absorption spectrum of **4** and the calculated spectrum of its computational model $[\kappa^2$-((Hpz)BHpz$_2$)Pt(H)(NCMe)$]^+$. (b) Experimental absorption spectrum of **6** and its computational model $[\kappa^2$-((Hpz)BHpz$_2$)Pt(μ-H)$]_2^{2+}$.

Table 6. Calculated Excitation Wavelengths and Relative Intensities (Relativistic).

excitation (wavelength, nm)	rel intensity
Monomer (**model-4**)	
321	0.41
310	3.99
308	0.34
304	0.65
Dimer (**model-6**)	
562	0.48
355	0.82
328	2.89

Figure 4 shows the experimental and computed absorption spectra, where Lorentzian functions have been scaled according to the computed relative intensities. Table 6 lists the calculated absorption wavelengths and their relative intensities. As anticipated, the quantitative agreement of the computed and observed spectra is poor. However, the calculation reveals an important qualitative difference between monomer **4** and dimer **6**: no absorption above 320 nm is predicted for **model-4**, whereas two low-energy absorptions (562 and 355 nm) are calculated for **model-6**.

Figure 5 shows 3D plots of the two electron-donating orbitals and the one accepting orbital of the two low-energy excitations in **model-6**. The transition at 562 nm is perhaps best characterized as a ligand-to-metal charge transfer (LMCT) excitation: the electron is elevated from an orbital with significant ligand

(87) Protonation of **2** with HBF_4 leads to the immediate formation of the deep purple hydride-bridged dimer. An intermediate solvent complex could not be observed by NMR.

(88) Ghosh, P.; Desrosiers, P. J.; Parkin, G. *J. Am. Chem. Soc.* **1998**, *120*, 10416.
(89) For an example of a recent study, see: Crespo, R.; Merchan, M.; Michl, J. *J. Phys. Chem. A* **2000**, *104*, 8593.
(90) Heinze, H. H.; Görling, A.; Rösch, N. *J. Chem. Phys.* **2000**, *113*, 2088.
(91) Casida, M. E.; Salahub, D. R. *J. Chem. Phys.* **2000**, *113*, 8918.

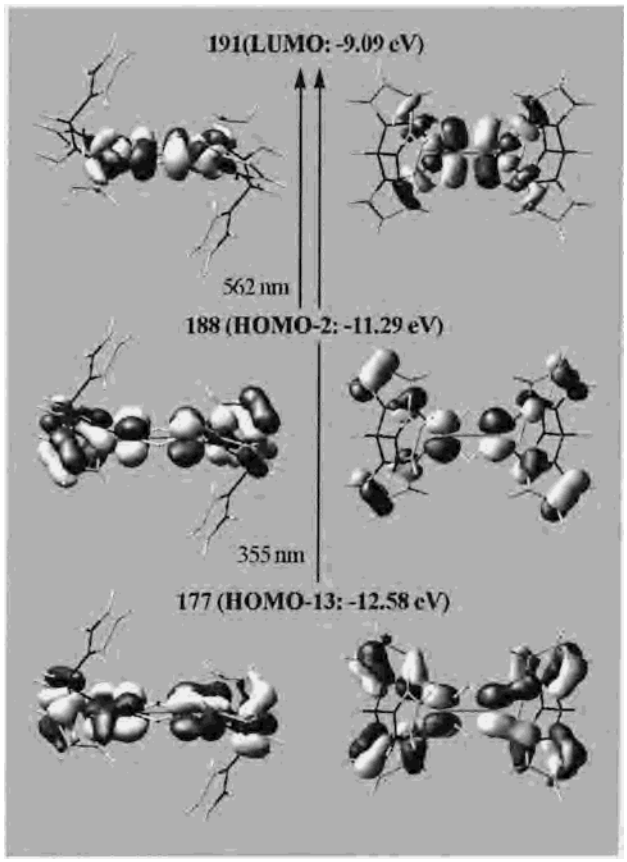

Figure 5. 3D plots of selected molecular orbitals of **model-6**. The orbital energies are given in parentheses. Two views of the same orbital are shown, respectively: The illustration on the right (top view) is related to the plot on the left (side view) by a rotation of 90° around the metal−metal vector.

character (MO-188) to a metal-dominated MO. MO-188 (HOMO-2) is metal−metal δ-antibonding in the Pt d_{yz} orbitals with a large out-of-phase contribution from the ligand π orbitals. The accepting orbital (MO-191) is the lowest unoccupied molecular orbital (LUMO) of the dimer, formally an out-of-phase combination of the Pt d_{xy} orbitals, which approximates the nonbonding combination of a 3-center-2-electron bond reminiscent of B_2H_6. A similar orbital is not available in the monomer model. The plots in Figure 5 show that the LUMO is mainly metal-based with significant out-of-phase contributions from the p orbitals of the directly coordinated nitrogen atoms. The second lowest excitation at 355 nm, for which the LUMO acts again as the charge-accepting orbital, has a charge-donating orbital, MO-177, somewhat similar to MO-188. MO-177 is also metal−metal d_{yz}-antibonding, but the metal−ligand interaction is in-phase, hence the lower energy of MO-177.

The orbitals involved in the lowest energy absorptions of the monomer $[\kappa^2$-((Hpz)BHpz$_2$)Pt(H)(NCMe)$]^+$ (**model-4**) are all MLCT bands involving transitions from platinum-based orbitals

(92) The orbital energy differences between the dimer and monomer make a quantitative analysis of the orbital energy shifts upon dimerization desirable in order to distinguish effects arising from the Tp ligand from those due to dimer formation. A discussion of the simple model systems $[Pt(H)_4]^{2-}$ and $[Pt_2(H)_6]^{2-}$ is given as Supporting Information.

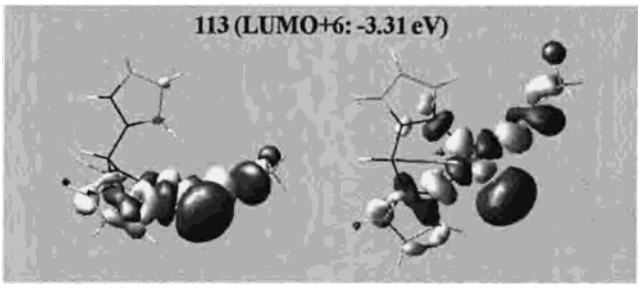

Figure 6. Lowest unoccupied molecular orbital (LUMO) of **model-4** showing significant Pt d atomic orbital character.

(d_{z^2}, d_{xz}, d_{yz}) to the LUMO+1 orbital, a ligand-based π orbital (see Supporting Information). Note the contrasting origins of the low-energy absorptions of **model-4** and **model-6**: none of the low-energy absorptions in **model-4** involves a transition to the metal center. In fact, the Pt d_{xy} based MO of the monomer which correlates with the dimer LUMO (Figure 6) is so high in energy that a transition from a Pt d_{yz} based MO (MO-104) to the Pt d_{xy} based MO (MO-113 = LUMO+6) would require a transition energy of 5.52 eV (corresponding to a 225 nm absorption band), if the transition were symmetry-allowed.[92]

Conclusion

The dihydridomethyl complex Tp′PtMe$(H)_2$ (**2**) was prepared from Tp′PtMe(CO) (**1**) in a basic acetone/water mixture by a slight modification of Keinan's procedure for TpPtMe$(H)_2$. Protonation of Tp′PtMe$(H)_2$ at a pyrazolyl ring promotes reductive elimination of methane, and the resulting platinum(II) monohydride intermediate can be trapped with acetonitrile or ethylene to yield chiral cationic complexes. The platinum(II) intermediate dimerizes in the absence of trapping ligand to form a dark-red dihydrido-bridged dimer **6** of C_{2h} symmetry, which was structurally characterized.

DFT calculations reproduce the structure of dimer **6** with two bridging hydride ligands. The electronic spectrum of the monomeric acetonitrile adduct **model-4** shows no absorption in the visible region below 321 nm, while low-energy absorptions at 562 and 355 nm are computed for dimer **model-6**. The two low-energy absorptions in dimer **model-6** involve transitions to a low-lying metal−metal nonbonding MO which is a central part of the 3-center-2-electron orbital scheme tying the Pt(μ-$H)_2$Pt entity together.

Acknowledgment. This work was supported by the National Science Foundation (Grant CHE-9727500) and the National Institutes of Health (Grant GM 28938). We thank Prof. H. Holden Thorp (UNC−Chapel Hill) for access to his UV/vis spectrometer. The North Carolina Supercomputing Center (NCSC) is gratefully acknowledged for providing computational time and technical assistance.

Supporting Information Available: Complete crystallographic data, in CIF format, for **4** and **6**. 3D plots of selected molecular orbitals of **model-4**. Electronic structure of the model systems $[PtH_4]^{2-}$ and $[Pt_2H_6]^{2-}$. This material is available free of charge via the Internet at http://pubs.acs.org.

IC010099Q